A Janus cobalt-based catalytic material for electro-splitting of water

Saioa Cobo, Jonathan Heidkamp, Pierre-André Jacques, Jennifer Fize, Vincent Fourmond, Laure Guétaz, Bruno Jousselme, Valentina Ivanova, Holger Dau, Serge Palacin, et al.

A Janus cobalt-based catalytic material for electro-splitting of water.

Saioa Cobo,[a] Jonathan Heidkamp,[b] Pierre-André Jacques,[a] Jennifer Fize,[a] Vincent Fourmond,[a] Laure Guetaz,[c] Bruno Jousselme,[d] Valentina Ivanova,[e] Holger Dau,[b] Serge Palacin,[d] Marc Fontecave[a, f] and Vincent Artero[*a]

[a] *Laboratoire de Chimie et Biologie des Métaux (CEA/Université Grenoble 1/CNRS), 17 rue des Martyrs, 38054 Grenoble cedex 09, France*

[b] *FB Physik, Free University Berlin, Arnimallee 14, D-14195 Berlin, Germany*

[c] *Institut LITEN, CEA LITEN/DTH/LCPEM, 17 rue des Martyrs, F-38054 Grenoble cedex 9, France*

[d] *CEA, IRAMIS, SPCSI, Chemistry of Surfaces and Interfaces group, F-91191 Gif sur Yvette Cedex, France*

[e] *CEA-Leti, MINATEC Campus, 17 rue des Martyrs, F-38054 Grenoble cedex 9, France*

[f] *Collège de France, 11 place Marcelin-Berthelot, 75231 Paris cedex 05, France.*

* To whom correspondence may be adressed. Fax: 0033 438789124; Tel: 0033 438789106; E-mail: vincent.artero@cea.fr

Exploitation of abundant but intermittent and diluted renewable energy sources, such as sunlight or wind,[1] requires efficient energy storage technologies. The cost-effective conversion of these energy sources into a chemical form via the production of a fuel is one of the greatest challenges of the century. Hydrogen is such a fuel which can be simply produced via water electrolysis, when the electricity is derived from renewable energy sources (photovoltaics, turbines…).[2] Promising devices, based on proton exchange membrane (PEM) technology, rely on the use of noble metal (Pt, Ir…)-based electrocatalysts but, due to the low abundance and consequent high cost of such precious metals, the long-term viability of these systems is questionable. Instead the transition to a Hydrogen economy requires the design and construction of efficient systems that utilize earth-abundant elements.[3] While important reports have been made recently regarding the use of cobalt,[4-12] nickel [13] and manganese[9,14] oxide materials as robust electrocatalysts for water oxidation (OER), few such materials exist for hydrogen evolution (HER).[15-18] We found that a robust nano-particulate electrocatalytic material, H_2-CoCat can be electrochemically prepared from aqueous cobalt salts in a phosphate

buffer. This material consists of metallic cobalt coated with a cobaltoxo/hydroxo-phosphate layer in contact with the electrolyte and mediates H_2 evolution from neutral aqueous buffer at modest overpotentials Remarkably, it can be converted upon anodic equilibration into the O_2-CoCat cobalt-oxide film[4] described by Kanan and Nocera catalysing O_2 evolution. The switch between the two catalytic forms is fully reversible and corresponds to a local interconversion between two morphologies and compositions at the surface of the electrode. After deposition, the noble-metal-free coating thus functions as a robust, bifunctional and switchable catalyst.

Innovative breakthroughs based on cobalt compounds appeared in the past decade[19] for electrocatalytic HER[4-8]. We[20-22] and others[23-25] reported that a series of cobaloxime and diimine-dioxime[21] compounds display remarkable properties for proton reduction with low overpotential requirements.[26] However, practical utilization of molecular catalysts requires their grafting with retention of the catalytic activity onto an electrode material,[16] which in the specific case of Co catalysts has so far been prevented by synthetic issues.[19] We thus turned toward a more direct and smoother method based on the reductive electrodeposition of a cobalt-based material, since this methodology recently proved successful for the preparation of MoS_2-[27,28] or NiMo-based materials[29,30] HER catalysts. We here establish that reduction of $Co(NO_3)_2{\cdot}6H_2O$ from an aqueous phosphate buffer (KPi, 0.5 mol.L^{-1}, pH 7) at a F-doped SnO_2 (FTO) electrode is a straightforward and highly convenient preparation of very stable electrocatalytic materials for H_2 evolution. Similar results are obtained if the water-soluble diimine dioxime cobalt(III) complex [Co(DO)(DOH)pnCl_2] ((DOH)(DOH)pn = N^2,$N^{2'}$-propanediylbis(2,3-butandione 2-imine 3-oxime); Figure S1) or the cobaloxime [Co($dmgBF_2$)$_2$(H_2O)$_2$] ($dmgH_2$ = dimethylglyoxime) are used as cobalt precursors under the same conditions.

Figure 1 reports the current densities obtained during a linear sweep voltammetry experiment (plain black trace, 0.05 mV.s^{-1}) of a $Co(NO_3)_2.6H_2O$ solution (0.5 mmol.L^{-1}) in KPi (0.5 mol.L^{-1}, pH 7) at an FTO electrode. A reductive process is observed with onset at –0.9 V vs Ag/AgCl. Simultaneous chromatographic monitoring of H_2 production (dotted black trace) indicates that no hydrogen is produced at this point. If the electrode potential is switched to more negative values (below –0.95 V vs Ag/AgCl) H_2 is produced. To provide more insights into the reductive process at work at the onset of the wave, we carried out an

electrolysis experiment at –0.9 V vs Ag/AgCl for 1 hour (Q=0.1 C.cm$^{-2}_{geometric}$), which resulted in a grey coating of the electrode. The scanning electronic micrograph (Figure 2a) shows isolated nanoparticles with an average ~10 nm in diameter. Performing the same electrolysis but at –1.0 V vs Ag/AgCl for 3 hours yields a film of ~2 μm thickness made from larger particles (100 nm) as shown by Figure 2b. During this experiment the current density stabilizes to a value of 2 mA.cm$^{-2}_{geometric}$. Neither the use of a longer electrolysis time nor a second electrolysis experiment in a new Co^{2+} solution could increase the current density. The modified electrode was then transferred to a Co-free KPi electrolyte and studied for its electrocatalytic properties under conditions described above. Figure 1 (red traces) reports current density (plain) and specific rate of H_2 evolution (dotted) traces as a function of the electrochemical potential values scaled versus the Reversible Hydrogen electrode (RHE), from which overpotential values can be directly obtained. Hydrogen evolution could be detected for overpotential values as low as 50 mV (Inset in Figure 1) and overpotential values of 270 mV and 385 mV are required to reach current density values of 0.5 and 2 mA.cm$^{-2}_{geometric}$ respectively. With such an electrode, the faradaic yield is found to be quantitative within the experimental accuracy. It should be noted that these overpotential values are much lower than those reported with cobalt-based molecular catalysts assayed under aqueous solutions. For instance, Co macrocycles generally require overpotentials of 500 mV to 700 mV[19] and a recently described pentadentate polypyridyl cobalt complex catalyzes H_2 evolution with onset of the catalytic current occurring for an overpotential of 660 mV.[31] Our catalytic material, hereafter named H_2-CoCat, appears to be stable as long as the electrode is kept at a potential more negative than about –0.6 V vs Ag/AgCl. When poised at a more positive potential, or left at open-circuit potential, the catalytic film readily dissolves in the electrolyte yielding Co(II) species. By ICP-MS titration of Co(II) ions in the electrolyte after full redissolution, we determine that 1.0 10^{-6} mol of cobalt are deposited per geometric cm^2, from which we derive an H_2-evolution turnover frequency of 80 h^{-1} per Co center at 385 mV overpotential.

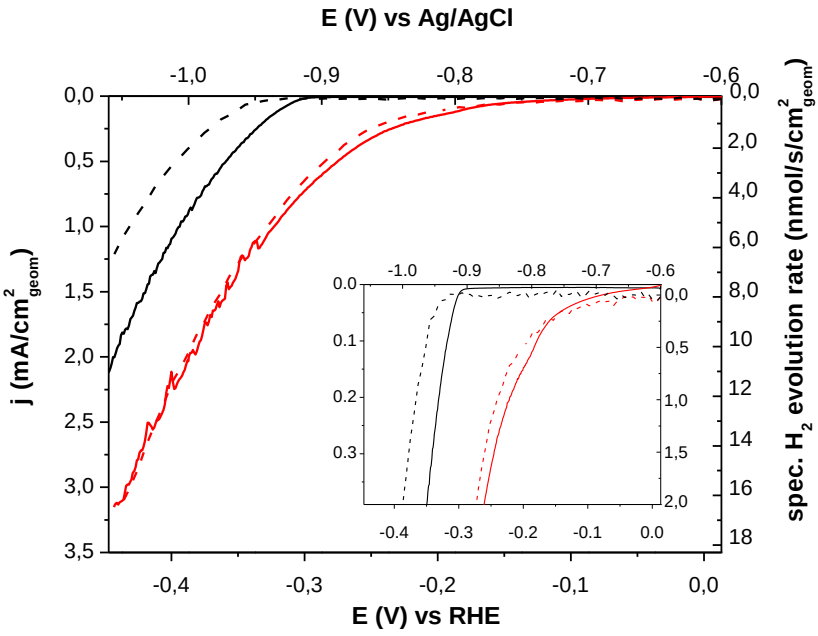
E (V) vs Ag/AgCl
-1,0
-0,9
-0,8
-0,7
-0,6
0,0
0,5
1,0
1,5
2,0
2,5
3,0
3,5
j (mA/cm²geom)
0,0
2,0
4,0
6,0
8,0
10
12
14
16
18
spec. H2 evolution rate (nmol/s/cm²geom)
-0,4
-0,3
-0,2
-0,1
0,0
E (V) vs RHE
-1.0
-0.9
-0.8
-0.7
-0.6
0.0
0.1
0.2
0.3
0,0
0,5
1,0
1,5
2,0
-0.4
-0.3
-0.2
-0.1
0.0

Figure 1. Linear voltammetry experiments. Black: current densities (plain) recorded at a FTO electrode (1 cm^2) in phosphate buffer (KPi, 0.5 $mol.L^{-1}$, pH 7) containing $Co(NO_3)_2.6H_2O$ (0.5 $mmol.L^{-1}$) at a low scan rate (0.05 $mV.s^{-1}$) with simultaneous GC monitoring of H_2 evolution (dotted): N_2 was continuously bubbled through the electrolyte at a constant flow (5 $mL.min^{-1}$) during the experiment and the concentration of H_2 in the output gas was determined every 2nd min by gas chromatography. This allowed determining the specific rate of H_2 evolution which is reported in the right scale. With the right and left scales used, superimposition of both current density and H_2 evolution rate traces shows quantitativity of the faradaic yield. Red: current densities (plain) and specific rate of H_2 evolution (dotted) recorded at a FTO electrode previously modified by controlled potential electrolysis for 3 h at –385 mV vs RHE in the Co-containing solution described above and then transferred into a cobalt-free buffer. Inset: blow-up of the low overpotential region showing evolution of H_2 with 50 mV onset overpotential.

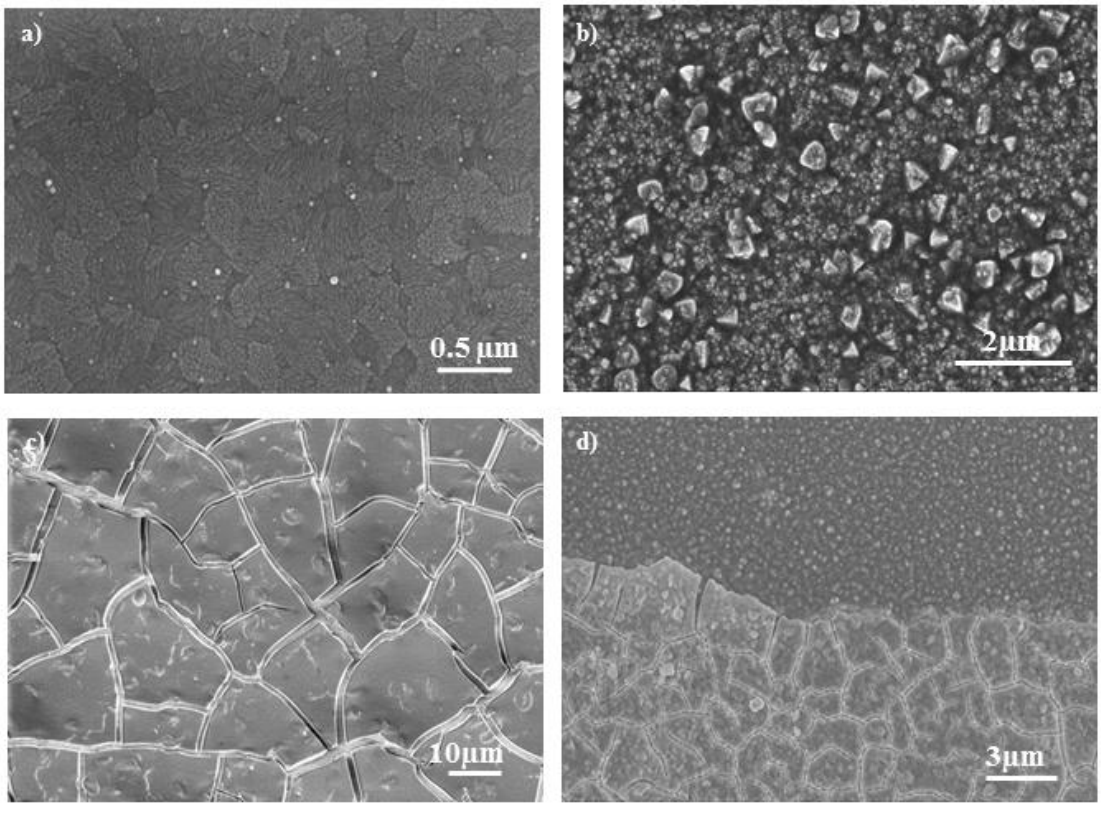

Figure 2. SEM images of electrodes modified by electrolysis at (a, left) –0.9 V vs Ag/AgCl for 1h ([Co(DO)(DOH)pnCl$_2$], 0.5 mmol.L^{-1}, ITO, 0.1 C.cm$^{-2}_{geometric}$) and (b, right) –1.0 V vs Ag/AgCl for 3h ($Co(NO_3)_2.6H_2O$ or [Co(DO)(DOH)pnCl$_2$], 0.5 mmol.L^{-1}, FTO, 6.5C.cm$^{-2}_{geometric}$) vs. RHE in phosphate buffer (KPi, 0.5 mol.L^{-1}, pH 7) containing; (c) SEM image of a H_2-CoCat film on FTO electrode equilibrated at 1.16 V vs Ag/AgCl for 90 min. in a cobalt-free 0.5 mol.L^{-1} KPi, pH 7 electrolyte (d) SEM image of H_2-CoCat film on FTO electrode initially equilibrated at –1.0 V Vs Ag/AgCl and taken out of the solution just after a potential switch to 1.16 V vs Ag/AgCl before equilibration of the current.

Figure 3 also shows that H_2-CoCat, displays much higher performances than a bulk cobalt foil. Tafel analysis (inset in Figure 3) gives a Tafel slope of 140 mV/decade and exchange current density of $10^{-5.5}$ A.cm$^{-2}_{geometric}$. This value is significantly higher than that found for metallic cobalt (10^{-6} A.cm$^{-2}_{geometric}$) or electrodeposited MoS_2 catalysts ($10^{-6.5}$ A.cm$^{-2}_{geometric}$).[28] NiMo-based materials exhibit current densities between 10^{-6} and 10^{-4} A.cm$^{-2}_{geometric}$.[30] We also compared H_2-CoCat with a similar cobalt coating described by Soto et al.[32] but deposited from NH_4Cl solution (pH 5.6) and with another nanoparticulate metallic Co coating reductively obtained from a Co^{2+}-containing $LiClO_4$ solution (pH 7).[33] Surface morphologies of the three samples were characterized using atomic force microscopy (Figure S6) and RMS roughness values of 87, 60 and 160 nm were determined for H_2-CoCat and the coatings deposited from NH_4Cl and $LiClO_4$ respectively. Cobalt quantification after oxidative dissolution of the films gave surface concentrations of 1.0 and 2.9 10^{-6} mol$_{Co}$.cm$^{-2}_{geometric}$ for the latter two samples respectively, in the range of that of_H_2-CoCat. Polarisation curves (Figure S4) show that H_2-CoCat is superior to the other two samples. This definitively speaks for H_2-CoCat being distinct in composition and intrinsically more active than previously described Co-based coatings. We note that molecular cobalt complexes combined with carbon–based materials also yield active electrocatalytic electrodes for H_2 evolution.[34,35] Yet these studies lack a detailed characterization of the surface state of the electrode material which would allow comparison with H_2-CoCat.

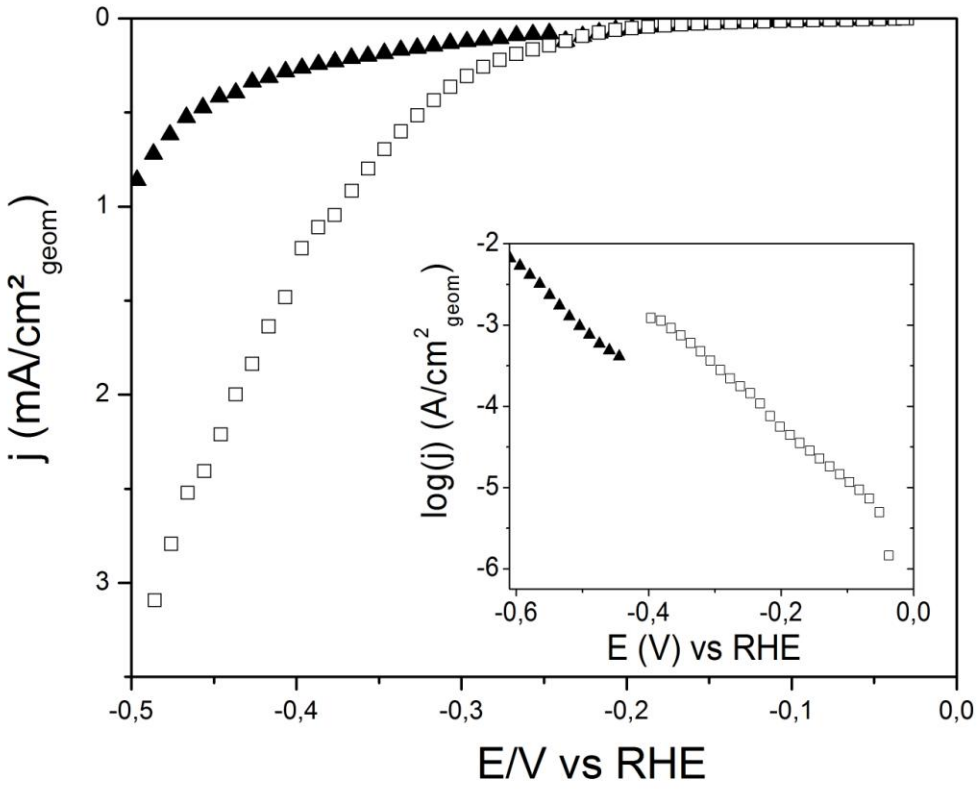

Figure 3. Linear voltammetry experiments recorded at a FTO electrode (1 cm^2) in phosphate buffer (KPi, 0.5 $mol.L^{-1}$, pH 7) at a low scan rate (0.05 $mV.s^{-1}$) for a FTO electrode modified with H_2-CoCat (□) and at a Co foil electrode (▲) Potentials have been converted to RHE. The corresponding Tafel plots are shown in the inset.

The structure of H_2-CoCat was characterized by X-ray photoelectron spectroscopy (XPS), Energy Dispersive X-ray (EDX) spectroscopy, X-ray absorption spectroscopy (XAS), in particular near-edge structure (XANES) and extended X-ray absorption fine-structure (EXAFS).

The XPS spectrum of freshly electro-deposited H_2-CoCat, recorded under limited air exposure conditions, shows the presence of cobalt, phosphorus and oxygen (Figure 4) and was comparable to that of commercially available $Co_3(PO_4)_2 \cdot xH_2O$. No significant signals are found in the N1s region when $[Co(DO)(DOH)pnCl_2]$ or $[Co(dmgBF_2)_2(H_2O)_2]$ are used as cobalt precursors confirming that the organic ligand is completely split up from with the cobalt ion during the cathodic deposition process. The P_{2p} region of both samples displays two sharp peaks with 133.4 eV and 134.4 eV binding energies (ratio of 2:1) corresponding to the $2p_{3/2}$ and $2p_{1/2}$ core levels of central phosphorus atom in phosphate species.[36] In the Co region, two broad sets of signals corresponding to $2p_{3/2}$ (782 eV) and $2p_{1/2}$ (798 eV) core levels are

observed, excluding the presence of metallic cobalt (778.0 eV) at the surface of the H_2-CoCat coating. O_{1s} signals are centered for both materials at 531.7 eV. P/Co/O ratios are however significantly different with a slight excess of cobalt and oxygen for H_2-CoCat (2:3.9:11.6) as compared to $Co_3(PO_4)_2 \cdot xH_2O$ (2:3:11.1). As the Co_{2p} and O_{1s} core levels binding energies[37] of cobalt oxides and hydroxides are in the same range as those of cobalt phosphate, we tentatively describe the surface of electrodeposited H_2-CoCat as a combination of cobalt(II) phosphate with a cobalt oxo/hydroxo species $Co_xO_y(OH)_z$, probably in the Co(II) state as observed for native cobalt oxide/hydroxide that forms at the surface of metallic cobalt.

EDX spectra (Fig. S2a) confirm the presence of Co, P and O together and additional signals arise from silicon and tin from FTO coated glass substrate. Since EDX, which probes deeply into the cathodically deposited film, indicates a Co/P ratio of 5:1, whereas XPS, which probes only a few nanometers below the surface, indicates a 1:2 Co/P ratio, we conclude that H_2-CoCat is not homogeneous in composition between bulk and surface.

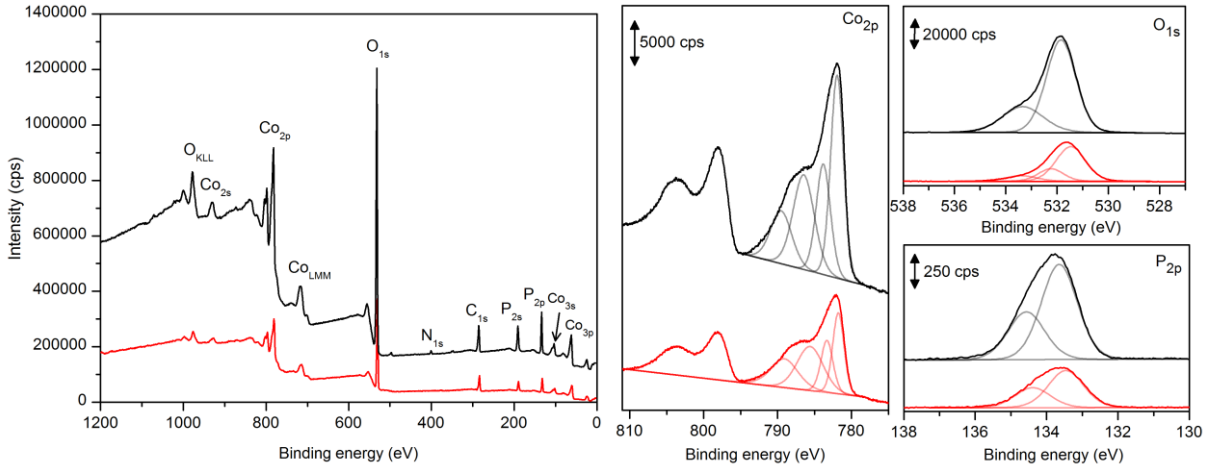

Figure 4: XPS survey (left), Co_{2p} (middle), O_{1s} (right up) and P_{2p} (right down) core levels spectra of H_2-CoCat deposited on FTO substrate (red) and commercial $Co_3(PO_4)_2 \cdot xH_2O$ (black).

The absence of crystalline features in the powder low-angle X-ray diffraction pattern recorded at low angles and in the electron diffraction patterns recorded in a transmission electron microscope indicates the amorphous nature of H_2-CoCat. For insight into the atomic structure, X-ray absorption spectra were collected at the Co *K*-edge after H_2-CoCat formation and fast freezing of the still-wet electrode in liquid nitrogen (quasi-in situ measurements).[7] When deposition (paralleled by catalytic H_2 evolution) was achieved at –1.0 V vs. Ag/AgCl, XANES and EXAFS measurements suggest a dominating contribution of the hexagonal close-packed phase of metallic cobalt (Fig. 5 and Fig. S3). However, the magnitude of EXAFS oscillation is by about 40% smaller than observed for a Co metal foil and furthermore the edge

spectra (inset in Figure 5) suggest a sizeable non-metallic contribution. An appropriate subtraction of the metallic contribution results in an EXAFS spectrum that suggests the presence of light atoms (O, N, C) in the first Co coordination sphere (Fig. S3d), but the determination of bond lengths by EXAFS simulations is prevented by noise in conjunction with uncertainties in the approach used to correct for the dominating contributions of the metallic cobalt.

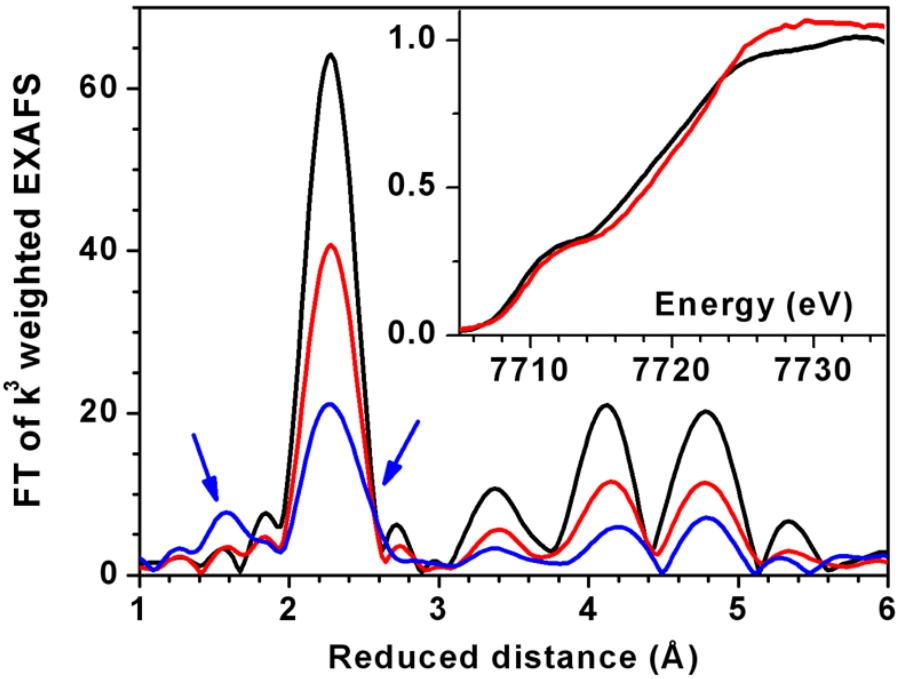

Figure 5. Fourier-transformed EXAFS spectra collected at the Co *K* edge. Red trace: H_2-CoCat equilibrated at –1.0 V vs Ag/AgCl. Blue trace: H_2-CoCat equilibrated at +1.16 V vs Ag/AgCl for 4 min. Black trace: Co metal foil (hexagonal close-packed state). The XANES spectra of the film formed at –1.0 V vs Ag/AgCl and of metallic cobalt are shown in the inset. The blue arrows mark features that are assignable to the contribution (~50%, Fig. S6) of a phase of edge-sharing CoO_6 octahedra to the spectrum of the film equilibrated at +1.16 V vs Ag/AgCl (blue line).

All these data indicate that the new material is made of nanoparticles with a cobalt oxo/hydroxo phosphate component mostly located at the surface and metallic cobalt in the bulk.

Poising the H_2-CoCat electrode at a fairly positive potential (+1.16 V vs. Ag/AgCl) resulted in a stable anodic current density of 1 $mA.cm^{-2}$ (Fig. S7) and concomitant oxygen evolution with quantitative faradaic yield. SEM observations of the electrode after 90 min

(Figure 2c) shows a homogeneous thin film, with cracks originated from drying, very similar to those obtained for the O_2-CoCat material (also named CoPi) reported in 2008 by Kanan and Nocera.[4,7]

In order to characterize the electrocatalytic material after this redox shift a detailed analysis by EDX, XPS and XAS has been carried out. According to EDX spectra (Fig S2b) the Co:P ratio is 1:2.5, which differs significantly from the 2:1 ratio previously reported for O_2-CoCat.[4] XPS analysis confirms the large phosphorus accumulation in the oxidized film (Fig S8). On the other hand, the XANES and EXAFS spectra (Fig. 4 and S9) of H_2-CoCat films equilibrated at +1.16 V vs. Ag/AgCl, indicate that about 50% of the Co film has undergone a transformation resulting in a Co oxide material, consisting of clusters of edge-sharing $Co^{III}O_6$ octahedra,[7,8,38] similar to that found in O_2-CoCat.

After cathodic deposition (black trace in Figure 6), alternate switches between oxidative (+1,775 V vs. RHE, blue traces in Figure 6) and reductive conditions (–385 mV vs. RHE, red traces in figure 6) show that the deposited material catalyzes both water oxidation and H_2 evolution respectively. Importantly we could not evidence any decrease in activity for both H_2 and O_2 evolution after several switches. From the current densities and chromatographic measurements, we derive turnover frequencies of 10 and 80 h^{-1} per Co center at 545 and 385 mV overpotential for O_2 and H_2 evolution respectively. We conclude that the material reported here enjoys a fast redox-dependent interconversion between the H_2-CoCat form and the O_2-CoCat form, catalytically competent for H_2 and O_2 evolution respectively. In order to determine whether this reversible transformation proceeds through the complete dissolution of one form of the CoCat film followed by the electrodeposition of the other form, we stopped the experiment before current stabilization after a switch from reductive to oxidative conditions. SEM analysis then reveals the coexistence of different domains at the surface of the electrode (Figure 2d) corresponding to both morphologies. This clearly stands for a progressive and local transformation of the material.

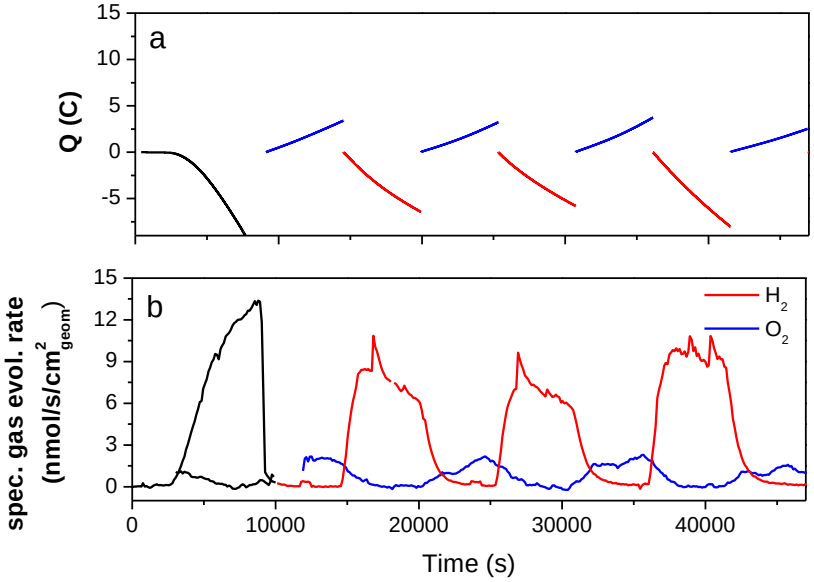

Figure 6. (a) Charge passed through a FTO electrode (1 cm^2) during controlled potential coulometry initially at –1.0 V vs. Ag/AgCl (3h, H_2-CoCat deposition) in 0.5 $mol.L^{-1}$ KPi, pH 7 electrolyte containing $Co(NO_3)_2.6H_2O$ (0.5 $mmol.L^{-1}$) and after transfer to a cobalt-free 0.5 $mol.L^{-1}$ KPi, pH 7 electrolyte, with potential switching between oxidative (blue, 1.16 V vs. Ag/AgCl) and reductive conditions (red, –1 V vs. Ag/AgCl); (b) Specific rates of hydrogen (red) and oxygen (blue) evolution quantified through gas chromatography measurements during the same experiment. N_2 was continuously bubbled through the electrolyte at a constant flow (5 $mL.min^{-1}$) during the experiment and the concentration of O_2 and H_2 in the output gas was determined every 2 min by gas chromatography.

First-row transition metals, namely Ni and Co, still display exchange current densities (<10^{-6} $A.cm^{-2}_{geometric}$) lower than those of platinum (10^{-3} $A.cm^{-2}_{geometric}$) for catalytic H_2 evolution (HER).[39,40] However Photo-Electro-Chemical (PEC) water-splitting devices require only low current densities (few $mA.cm^{-2}_{geometric}$[29,41-43]) since their activity is limited by the photon flux from the sun but must be made from abundant and cheaply processed materials both for light harvesting[18,44,45] and catalysis (both HER[18,30] and OER[46,47]) to be economically viable. Oxidatively (O_2-CoCat[4]) or reductively (MoS_2-[27,28], NiMo-based materials[29,30]) deposited OER and HER catalysts are fulfilling such requirements and are thus potential alternatives to platinum. Further investigation of new compositions and new nanostructures based on abundant metals should thus provide improved electrocatalytic materials. We report here a new HER electrocatalytic material for such applications, namely H_2-CoCat consisting of metallic cobalt coated with a cobalt oxo/hydroxo phosphate layer, as shown from detailed spectroscopic and microscopic characterizations with catalytic performances significantly improved with respect to metallic cobalt.

H_2-CoCat is remarkable for the following reasons. First, it is easily prepared by

electroreduction of simple divalent cobalt salts. Second, H_2-CoCat is a robust and active electrocatalytic material for hydrogen evolution working at low overpotentials (>50 mV) and under strictly neutral conditions. Third, it can be converted upon anodic equilibration into the O_2-CoCat cobalt-oxide film[4] catalysing O_2 evolution. The switch between the two catalytic forms is fully reversible and corresponds to a local interconversion between two morphologies at the surface of the electrode and two types of non-metallic atomic structures. After deposition, the coating thus functions as a robust, bifunctional and switchable catalyst. To the best of our knowledge, comparable properties have never been observed yet for any non-noble metal catalyst.

This behaviour is possible because such electrodeposited materials are in equilibrium with solution metal ions, depending on the applied electrochemical potential. This has the advantage of allowing self-repair to take place as demonstrated by D. Nocera for O_2-CoCat.[4] In that specific case, Co^{2+} ions are released in the solution at mild potential and can be redeposited under strong anodic conditions. We show here that these Co^{2+} ions can also be redeposited under cathodic conditions, but now forming H_2-CoCat. This process is reversible and O_2-CoCat can be prepared either from H_2-CoCat or by anodic oxidation of metallic cobalt.[48] These findings thus open up new possibilities with respect to simple and simultaneous electrodeposition of OER and HER catalysts from the same phosphate-buffered electrolyte, as well as self-repair at both electrodes. This could work in an artificial-leaf device,[29,41-43] even in the absence of a proton-conducting membrane separating (photo)anode and (photo)cathode (e.g., substitution of expensive Nafion membranes by an inexpensive mesh for separation of gas bubbles). Such an ingeniously simple approach may also be applicable toward photo-electrodeposition on heterogeneous semiconductor nanoparticles.[49,50]

Methods

Before starting the deposition, the FTO substrate is cycled hundreds of times between –1 V and +1 V in 0.5 M potassium phosphate buffer (KPi), pH 7.0 to ensure the stability and reproducibility of experiments. Catalyst films were grown by controlled potential electrolysis of freshly prepared 0.5 mM $Co(NO_3)_2$ solution and in 0.5 M KPi, pH 7.0. Performing the electrolysis at –1V (vs Ag/AgCl) gives rise to a catalyst film of several micrometer thickness formed by nanoparticles after a course of around three hours. During this time, a film is formed on the working electrode surface. After the film formation is completed, the substrate

is transferred to a cobalt-free 0.5 M KPi, pH 7.0, with potential switching between oxidative (+1.16 V vs. Ag/AgCl) and reductive conditions (–1 V vs. Ag/AgCl).

Authors contributions: V. A. and M. F. designed research; S. C., V. F., P.-A. J., J. F., V. I. and V. A. performed research; J. H. and H. D. performed X-ray absorption spectroscopy studies; B. J. and S. P. performed X-ray photoelectron spectroscopy studies; L. G. and S. C. performed Scanning Electronic microscopy measurements and surface Energy Dispersive X-ray analysis; V. A. wrote the paper.

The authors declare no conflict of interest.

Acknowledgments

The authors thank P. Jegou for XPS measurements, Bernard Sartor for the design and construction of a specific electrochemical cell allowing working with FTO-coated glass electrodes, P. Chernev, K. Klingan, M. Risch and I. Zaharieva (FU Berlin) as co-workers during the XAS measurements at the KMC-1 beamline of the BESSY synchrotron (Helmholtz Zentrum Berlin, HZB) which were technically supported by F. Schäfers and M. Mertin (HZB). Financial support by the Nanosciences Program of CEA (Grant Nanocat'O_2), the UniCat cluster of excellence (Unifying Concepts in Catalysis, Berlin) and the European Commission (7th Framework Programme, SOLAR-H2, grant # 212508) is gratefully acknowledged.

References

1. Lewis, N.S. & Nocera, D.G. Powering the planet: Chemical challenges in solar energy utilization. *Proc. Natl. Acad. Sci. USA* **104**, 20142-20142 (2007).
2. Armaroli, N. & Balzani, V. The Hydrogen Issue. *ChemSusChem* **4**, 21-36 (2011).
3. Gordon, R.B., Bertram, M. & Graedel, T.E. Metal stocks and sustainability. *Proc. Natl. Acad. Sci. USA* **103**, 1209-1214 (2006).
4. Kanan, M.W. & Nocera, D.G. In situ formation of an oxygen-evolving catalyst in neutral water

containing phosphate and Co^{2+}. *Science* **321**, 1072-1075 (2008).
5. Jiao, F. & Frei, H. Nanostructured Cobalt Oxide Clusters in Mesoporous Silica as Efficient Oxygen-Evolving Catalysts. *Angew. Chem. Int. Ed.* **48**, 1841-1844 (2009).
6. Yin, Q.S. et al. A Fast Soluble Carbon-Free Molecular Water Oxidation Catalyst Based on Abundant Metals. *Science* **328**, 342-345 (2010).
7. Risch, M. et al. Cobalt-Oxo Core of a Water-Oxidizing Catalyst Film. *J. Am. Chem. Soc.* **131**, 6936-6937 (2009).
8. Dau, H. et al. The Mechanism of Water Oxidation: From Electrolysis via Homogeneous to Biological Catalysis. *ChemCatChem* **2**, 724-761 (2010).
9. Jiao, F. & Frei, H. Nanostructured cobalt and manganese oxide clusters as efficient water oxidation catalysts. *Energy Environ. Sci.* **3**, 1018-1027 (2010).
10. Shevchenko, D., Anderlund, M.F., Thapper, A. & Styring, S. Photochemical water oxidation with visible light using a cobalt containing catalyst. *Energy Environ. Sci.* **4**, 1284-1287 (2011).
11. Wee, T.-L. et al. Photochemical Synthesis of a Water Oxidation Catalyst Based on Cobalt Nanostructures. *J. Am. Chem. Soc.* **133**, 16742-16745 (2011).
12. Chou, N.H., Ross, P.N., Bell, A.T. & Don Tilley, T. Comparison of Cobalt-based nanoparticles as Electrocatalysts for Water Oxidation. *ChemSusChem* **11**, 1566-1569 (2011).
13. Dinca, M., Surendranath, Y. & Nocera, D.G. Nickel-borate oxygen-evolving catalyst that functions under benign conditions. *Proc. Natl. Acad. Sci. USA* **107**, 10337-10341 (2010).
14. Zaharieva, I. et al. Synthetic manganese-calcium oxides mimic the water-oxidizing complex of photosynthesis functionally and structurally. *Energy Environ. Sci.* **4**, 2400-2408 (2011).
15. Tran, P.D. et al. Noncovalent Modification of Carbon Nanotubes with Pyrene-Functionalized Nickel Complexes: Carbon Monoxide Tolerant Catalysts for Hydrogen Evolution and Uptake. *Angew. Chem. Int. Ed.* **50**, 1371-1374 (2011).
16. Le Goff, A. et al. From Hydrogenases to Noble Metal-Free Catalytic Nanomaterials for H_2 Production and Uptake. *Science* **326**, 1384-1387 (2009).
17. Merki, D. & Hu, X. Recent developments of molybdenum and tungsten sulfides as hydrogen evolution catalysts. *Energy Environ. Sci.* **4**, 3878-3888 (2011).
18. Hou, Y.D. et al. Bioinspired molecular co-catalysts bonded to a silicon photocathode for solar hydrogen evolution. *Nat. Mater.* **10**, 434-438 (2011).
19. Artero, V., Chavarot-Kerlidou, M. & Fontecave, M. Splitting water with cobalt. *Angew. Chem. Int. Ed.* **50**, 7238-7266 (2011).
20. Baffert, C., Artero, V. & Fontecave, M. Cobaloximes as functional models for hydrogenases. 2. proton electroreduction catalyzed by difluoroborylbis(dimethylglyoximato)cobalt(II) complexes in organic media. *Inorg. Chem.* **46**, 1817-1824 (2007).
21. Jacques, P.-A., Artero, V., Pécaut, J. & Fontecave, M. Cobalt and nickel diimine-dioxime complexes as molecular electrocatalysts for hydrogen evolution with low overvoltages. *Proc. Natl. Acad. Sci. U.S.A.* **106**, 20627-20632 (2009).
22. Razavet, M., Artero, V. & Fontecave, M. Proton electroreduction catalyzed by cobaloximes: Functional models for hydrogenases. *Inorg. Chem.* **44**, 4786-4795 (2005).
23. Dempsey, J.L., Winkler, J.R. & Gray, H.B. Mechanism of H_2 Evolution by a Photogenerated Hydridocobaloxime. *J. Am. Chem. Soc.* **132**, 16774-16776 (2010).
24. Hu, X.L., Cossairt, B.M., Brunschwig, B.S., Lewis, N.S. & Peters, J.C. Electrocatalytic hydrogen evolution by cobalt difluoroboryl-diglyoximate complexes. *Chem. Commun.*, 4723-4725 (2005).
25. Hu, X., Brunschwig, B.S. & Peters, J.C. Electrocatalytic hydrogen evolution at low overpotentials by cobalt macrocyclic glyoxime and tetraimine complexes. *J. Am. Chem. Soc.* **129**, 8988-8998 (2007).
26. Fourmond, V., Jacques, P.A., Fontecave, M. & Artero, V. H_2 Evolution and Molecular Electrocatalysts: Determination of Overpotentials and Effect of Homoconjugation. *Inorg. Chem.* **49**, 10338-10347 (2010).
27. Merki, D., Fierro, S., Vrubel, H. & Hu, X.L. Amorphous molybdenum sulfide films as catalysts for electrochemical hydrogen production in water. *Chemical Science* **2**, 1262-1267 (2011).
28. Jaramillo, T.F. et al. Identification of active edge sites for electrochemical H_2 evolution from MoS_2 nanocatalysts. *Science* **317**, 100-102 (2007).
29. Reece, S.Y. et al. Wireless Solar Water Splitting Using Silicon-Based Semiconductors and Earth-Abundant Catalysts. *Science* **334**, 645-648 (2011).
30. McKone, J.R. et al. Evaluation of Pt, Ni, and Ni-Mo electrocatalysts for hydrogen evolution on crystalline Si electrodes. *Energy Environ. Sci.* **4**, 3573-3583 (2011).
31. Sun, Y. et al. Molecular Cobalt Pentapyridine Catalysts for Generating Hydrogen from Water. *J. Am. Chem. Soc.* **133**, 9212-9215 (2011).

32. Soto, A.B., Arce, E.M., PalomarPardave, M. & Gonzalez, I. Electrochemical nucleation of cobalt onto glassy carbon electrode from ammonium chloride solutions. *Electrochim. Acta* **41**, 2647-2655 (1996).
33. Cui, C.Q., Jiang, S.P. & Tseung, A.C.C. Electrodeposition of Cobalt from Aqueous Chloride Solutions. *J. Electrochem. Soc.* **137**, 3418-3423 (1990).
34. Pantani, O., Anxolabehere-Mallart, E., Aukauloo, A. & Millet, P. Electroactivity of cobalt and nickel glyoximes with regard to the electro-reduction of protons into molecular hydrogen in acidic media. *Electrochem. Commun.* **9**, 54-58 (2007).
35. Berben, L.A. & Peters, J.C. Hydrogen evolution by cobalt tetraimine catalysts adsorbed on electrode surfaces. *Chem. Commun.* **46**, 398-400 (2010).
36. Hu, G.-R., Deng, X.-R., Peng, Z.-D. & Du, K. Comparison of $AlPO_4^-$ and $Co_3(PO_4)_2^-$coated $LiNi_{0.8}Co_{0.2}O_2$ cathode materials for Li-ion battery. *Electrochim. Acta* **53**, 2567-2573 (2008).
37. Yang, J., Liu, H., Martens, W.N. & Frost, R.L. Synthesis and Characterization of Cobalt Hydroxide, Cobalt Oxyhydroxide, and Cobalt Oxide Nanodiscs. *J. Phys. Chem. C* **114**, 111-119 (2009).
38. Kanan, M.W. et al. Structure and Valency of a Cobalt−Phosphate Water Oxidation Catalyst Determined by in Situ X-ray Spectroscopy. *J. Am. Chem. Soc.* **132**, 13692-13701 (2010).
39. Trasatti, S. Work Function, Electronegativity, and Electrochemical Behavior of Metals .3. Electrolytic Hydrogen Evolution in Acid Solutions. *J. Electroanal. Chem.* **39**, 163-& (1972).
40. Miles, M.H. Evaluation of Electrocatalysts for Water Electrolysis in Alkaline-Solutions. *J. Electroanal. Chem.* **60**, 89-96 (1975).
41. Khaselev, O. & Turner, J.A. A monolithic photovoltaic-photoelectrochemical device for hydrogen production via water splitting. *Science* **280**, 425-427 (1998).
42. Rocheleau, R.E., Miller, E.L. & Misra, A. High-efficiency photoelectrochemical hydrogen production using multijunction amorphous silicon photoelectrodes. *Energy Fuels* **12**, 3-10 (1998).
43. Yamada, Y. et al. One chip photovoltaic water electrolysis device. *Int. J. Hydrogen Energy* **28**, 1167-1169 (2003).
44. Sivula, K., Le Formal, F. & Gratzel, M. Solar Water Splitting: Progress Using Hematite (alpha-Fe_2O_3) Photoelectrodes. *Chemsuschem* **4**, 432-449 (2011).
45. Paracchino, A., Laporte, V., Sivula, K., Gratzel, M. & Thimsen, E. Highly active oxide photocathode for photoelectrochemical water reduction. *Nat. Mater.* **10**, 456-461 (2011).
46. Pijpers, J.J.H., Winkler, M.T., Surendranath, Y., Buonassisi, T. & Nocera, D.G. Light-induced water oxidation at silicon electrodes functionalized with a cobalt oxygen-evolving catalyst. *Proc. Natl. Acad. Sci. USA* **108**, 10056-10061 (2011).
47. Zhong, D.K., Cornuz, M., Sivula, K., Graetzel, M. & Gamelin, D.R. Photo-assisted electrodeposition of cobalt-phosphate (Co-Pi) catalyst on hematite photoanodes for solar water oxidation. *Energy Environ. Sci.* **4**, 1759-1764 (2011).
48. Young, E.R., Nocera, D.G. & Bulovic, V. Direct formation of a water oxidation catalyst from thin-film cobalt. *Energy Environ. Sci.* **3**, 1726-1728 (2010).
49. Maeda, K., Higashi, M., Lu, D.L., Abe, R. & Domen, K. Efficient Nonsacrificial Water Splitting through Two-Step Photoexcitation by Visible Light using a Modified Oxynitride as a Hydrogen Evolution Photocatalyst. *J. Am. Chem. Soc.* **132**, 5858-5868 (2010).
50. Maeda, K. et al. Photocatalyst releasing hydrogen from water - Enhancing catalytic performance holds promise for hydrogen production by water splitting in sunlight. *Nature* **440**, 295-295 (2006).